JMEPEG (2012) 21:2345–2353
DOI: 10.1007/s11665-012-0169-4

1059-9495/$19.00

Enhanced Fatigue Crack Propagation Resistance in an Al-Zn-Mg-Cu Alloy by Retrogression and Reaging Treatment

Xu Chen, Zhiyi Liu, Mao Lin, Ailin Ning, and Sumin Zeng

(Submitted December 8, 2011; in revised form January 15, 2012)

The microstructures and fatigue crack propagation (FCP) behavior of an Al-Zn-Mg-Cu alloy in T761 and retrogression and reaging (RRA) conditions were characterized by employing differential scanning calorimetry, optical microscopy, scanning electron microscopy, transmission electron microscopy, and electron backscatter diffraction. The results suggested that coarse η′ precipitates were present in T761-treated sample, while fine dispersed η′ precipitates and GP zones were uniformly distributed in RRA-treated ones. Besides, the width of precipitate-free zones (PFZs) in T761-treated sample was found to be much greater than that in RRA-treated ones. Compared with T761-treated sample, the enhanced FCP resistance of RRA-treated sample was attributed to the shearable particles in matrix and narrow PFZs.

Keywords Al-Zn-Mg-Cu alloy, fatigue, microstructures, retrogression and reaging

1. Introduction

Al-Zn-Mg-Cu alloys have been used widely for structural applications in aerospace industry due to their excellent mechanical properties, which are greatly influenced by fine precipitates and its precursors (Ref 1, 2). The upper wing skin material is one of the most significant applications of the Al-Zn-Mg-Cu alloy in aeroplane. High strength, excellent corrosion resistance, and fatigue resistance are particularly required for the material (Ref 3-6). The overaging heat treatment T7 has been traditionally applied to reduce the susceptibility of Al-Zn-Mg-Cu alloy to stress corrosion cracking (SCC). This heat treatment, however, necessarily leads to a sacrifice of the maximum strength of the alloy. To satisfy those requirements, a three-step heat treatment, called retrogression and reaging (RRA) treatment, was devised by Cina (Ref 7) and it was claimed to increase dramatically the SCC resistance of the material without sacrificing its maximum strength.

RRA heat treatment consists of retrogressing the T6 materials at a high temperature for a short time and reaging the retrogressed materials at a lower temperature. During the retrogression step an initial reduction in hardness was observed. The time corresponding to minimum hardness in retrogression curve was originally thought to be an optimum time for the retrogression treatment, producing the best combination of strength and resistance to SCC. Danh et al. (Ref 8) indicated that the reduction in strength observed during the initial stage of retrogression was ascribed to the partial dissolution of GP zones, while a TEM study in 7075-T6 alloy by Park and Ardell (Ref 9, 10) revealed the reduction was due to the dissolution of η′ precipitates. Viana et al. (Ref 11) have studied the microstructure of 7075 alloy and proposed that the dissolution of the less stable particles, GP zones and smaller η′ precipitates, occurred during retrogression stage.

Several works have focused on the influence of RRA treatment on corrosion resistance. Knight et al. (Ref 12) revealed that there was a significantly higher copper content of grain boundary precipitates (GBPs) in the overaged alloys with the lower SCC susceptibilities. Hence, it seems likely that the SCC susceptibility is controlled by grain boundary microchemistry, such as GBPs composition. Those were in agreement with Peng et al. (Ref 13) who proposed that SCC resistance increased with the increase of copper content of GBPs. Similar phenomena have been observed in Ref 14, where the retrogression and reaged material had a matrix richer in Zn, and precipitates richer in Cu, as compared with the peakaged material. For the AA7050 alloy in RRA condition, Oliveira et al. (Ref 15) found that the SCC performance was close to the T7 condition. Li et al. (Ref 16) also researched the exfoliation corrosion behavior of the RRA-treated alloy AA7150 and concluded that its exfoliation corrosion rating was similar to that of the T7 condition.

As one of the most important properties, investigations related to fatigue resistance of the overaged Al-Zn-Mg-Cu alloys have been studied for many years (Ref 17-19), but little attention has been paid on the effect of RRA treatment on fatigue behavior of Al-Zn-Mg-Cu alloys. Srivatsan et al. (Ref 20) discussed the influence of elevated temperature on the stress amplitude-controlled fatigue response and concomitant fatigue life, deformation, and fracture characteristics of alloy 7055-T7751.

Xu Chen, Zhiyi Liu, Mao Lin, and **Sumin Zeng**, Key Laboratory of Nonferrous Metal Materials Science and Engineering, Ministry of Education, Central South University, Changsha 410083, China and School of Material Science and Engineering, Central South University, Changsha 410083, China; and **Ailin Ning**, Department of Mechanical Engineering, Shaoyang University, Shaoyang 422000, China. Contact e-mail: liuzhiyi335@163.com.

However, it is worth of noting that the T7751 treatment involves solution heat treatment, water quench, and a permanent stretch prior to artificial aging at 190 °C, which is different from the RRA treatment proposed by Cina (Ref 7). Chen et al. (Ref 21) studied the effects of precipitates on the fatigue crack propagation (FCP) rate of AA7055 alloy subjected to different aging treatments, whereas the influence of the width of precipitate-free zones (PFZs) is not mentioned. Furthermore, no examination was performed on the fatigue fracture surfaces to clarify the relationship between microstructures and fatigue fracture behavior. Previous study of an Al-5.9Zn-2.6Mg-1.7Cu alloy revealed that FCP resistance was observed to be significantly higher for underaged microstructures containing shearable precipitates in comparison to overaged condition with unshearable precipitates (Ref 18). Desmukh et al. (Ref 19) also found that the FCP rate of the overaged 7010 alloy was higher than that of the peakaged alloy. So far, however, no previous work focused on the comparisons of fatigue behavior between the Al-5.5Zn-2.3Mg-1.5Cu alloy in T761 and RRA conditions. In this study, therefore, the FCP rates of the alloy in both conditions were measured. The fatigue fracture behavior of the alloy in both conditions was also analyzed in detail.

2. Experimental Procedures

The investigations were carried out on the alloy of composition 5.5 wt.% Zn, 2.3 wt.% Mg, 1.5 wt.% Cu, 0.21 wt.% Cr, 0.04 wt.% Mn, 0.03 wt.% Ti, 0.03 wt.% Fe, 0.03 wt.% Si, and balance Al. The material was received as a 3 mm thickness plate. All the samples were solution-treated at 470 °C for 1 h and cold water quenched. For the T761 condition, the quenched samples were immediately stretched with 2% and then experienced a duplex aging treatment (aged at 125 °C for 3 h and then 170 °C for 10 h in air furnace). The RRA treatment was applied to the T6 material (the quenched samples were aged at 120 °C for 25 h). The retrogression treatment on the strips was performed in an oil bath at 190 °C, which was determined by the result of differential scanning calorimetry (DSC). The strips were retrogressed for 10 min and water quenched to room temperature. Reaging treatment was immediately carried out similar to the T6 treatment, namely 25 h at 120 °C, after the retrogression treatment.

The tensile properties of the samples with gauge length of 30 mm were evaluated with a CSS 44100 universal testing machine at room temperature in long transverse (LT) direction with 2 mm/min loading speed. A TecnaiG^{2}20 transmission electron microscopy (TEM) with an operating voltage of 200 kV, together with selected area electron diffraction (SAED) was utilized to characterize the microstructures of the samples in both conditions. Slices for TEM test were cut directly from samples, and subsequently were ground to 100 μm and punched into 3 mm disc. The electrolyte was a mixture of 70% methanol and 30% nitric acid, and thinning was performed at −25 °C. Samples for optical microscopy observation were prepared by conventional mechanical polishing and subsequent etching with Keller's reagent. DSC experiment was carried out using a NETZSCH SAT 449C calorimeter.

FCP test was performed on compact tension samples taken from the plates in the LT orientation with a size of 45.6 × 38 × 3 mm (L × W × B) to obtain the FCP rates. All FCP tests were conducted at a stress ratio ($R = K_{min}/K_{max}$) of 0.1 with a sine-wave loading frequency of 10 Hz on an MTS machine at room temperature and laboratory air environment. Fatigue fracture surfaces were analyzed by a FEI Quanta 200 scanning electron microscope (SEM) with the operating voltage of 15 kV. Fatigued samples with both conditions were unloaded at high ΔK regime to detect the crack propagation path by electron backscatter diffraction (EBSD) method. The preparation of samples for EBSD studies consisted of conventional mechanical grind and followed by electropolishing. The samples were electropolished in a solution consisting of 10% perchloric acid and 90% ethanol at 18-23 V for 10-20 s. EBSD measurements were performed in a Sirion 200 field emission gun scanning electron microscope with the accelerating voltage of 20 kV.

3. Results

3.1 Microstructures and Mechanical Properties

Representative TEM micrographs and corresponding SAED patterns of the microstructures in T761 and RRA conditions are shown in Fig. 1. The precipitates distributed homogeneously in the aluminum matrix. It can be observed that the precipitates in RRA-treated sample are much finer and more dispersed than that in T761-treated sample. The SAED patterns in ⟨001⟩ Al projection are represented in Fig. 1(a) and (c). The strong diffraction spots at 1/3 and 2/3 of $\{220\}_{Al}$ indicate the presence of η′ precipitates. Therefore, the dominant strengthening particles are η′ precipitates in the both samples. Figure 1(b) and (d) shows that grain boundaries are decorated intermittently by equilibrium η precipitates. This is to be expected in general because the velocity of solute diffusivity is greater at grain boundaries than that in grain interiors, allowing more rapid growth of precipitates. The formation of GBPs leads to the depletion of solute atoms and vacancies near the grain boundary and consequent formation of PFZs. It is apparent that the width of PFZs in T761-treated sample is much greater than that in RRA-treated ones. Tensile properties of the samples in T6, T761, and RRA conditions at room temperature are listed in Table 1. The tensile properties of RRA-treated sample, which are closely comparable to those of T6-treated ones, are greatly improved compared with those of T761-treated sample.

T6 material shows a homogeneous distribution of fine particles in the matrix, as shown in Fig. 2(a). Figure 3 shows the DSC scan on the T6 material, suggesting that the endothermic peak sited at 189 °C is ascribed to the dissolution of unstable particles. The micrographs of T6 material retrogressed for 10 min at 190 °C are shown in Fig. 2(c), indicating a noticeable decrease in volume fraction of the particles due to the dissolution of unstable particles during retrogression treatment, which is confirmed in Fig. 3. According to the analysis of SAED patterns shown in Fig. 2(c), the undissolved particles in the retrogressed sample are η′ precipitates. The dissolution of the particles enriches the matrix in Zn and Mg, which in turn promotes the nucleation and growth of particles during reaging treatment. Therefore, it should be added that GP zones would also be expected besides the presence of fine η′ precipitates in the RRA-treated sample shown in Fig. 1(c) as proposed by Danh et al. (Ref 8). TEM investigations were also carried out on the precipitates at grain boundaries shown in Fig. 2(b) and (d), and suggesting a coarsening behavior of GBPs during retrogression treatment. Besides, PFZs are found to form during retrogression treatment.

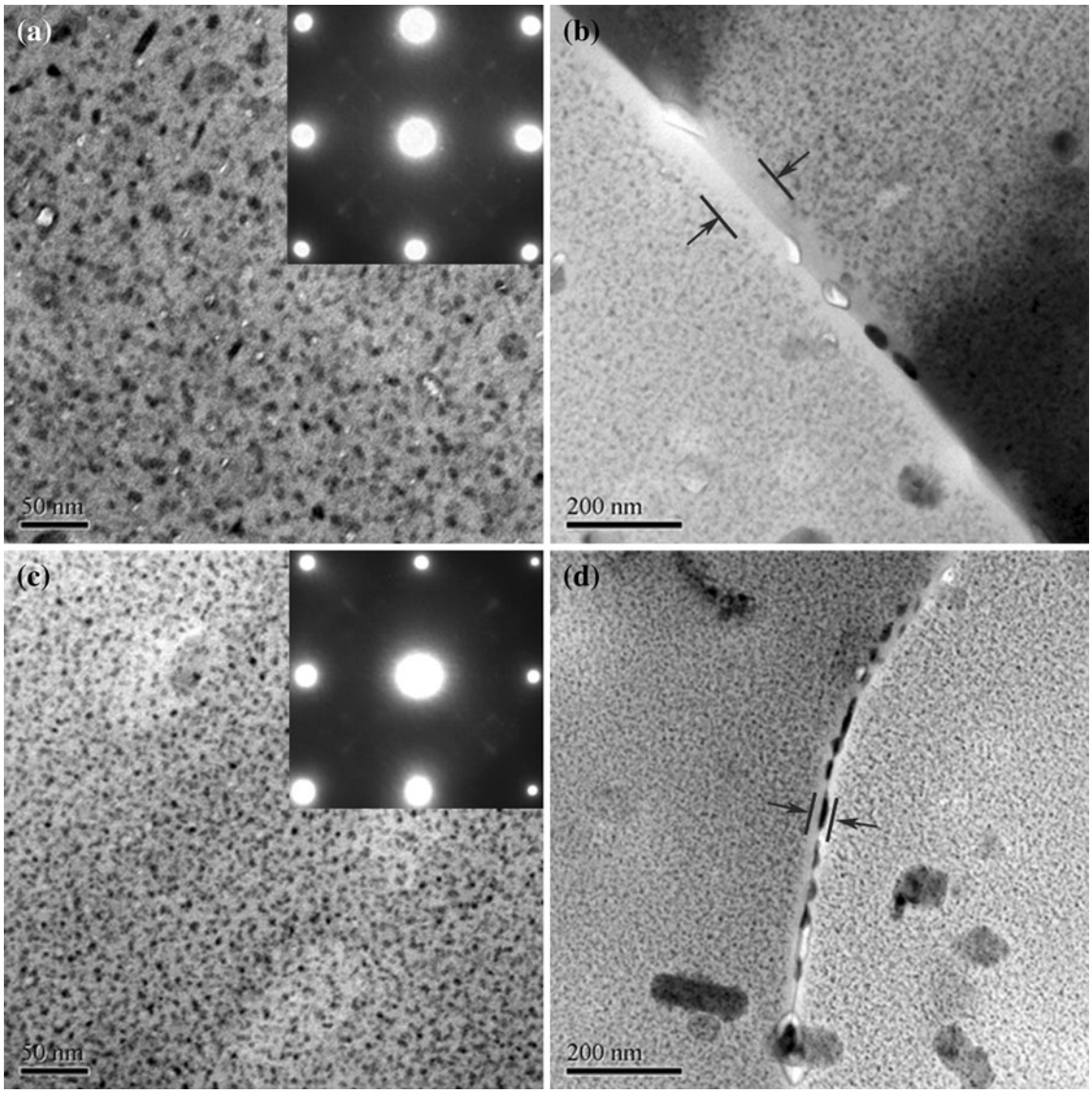

Fig. 1 TEM micrographs and corresponding SAED patterns of the alloy in various conditions. (a, b) T761 and (c, d) RRA

Table 1 Tensile properties of the Al-Zn-Mg-Cu alloy in T6, T761, and RRA conditions at room temperature

Condition	Ultimate strength, MPa	Yield strength, MPa	Elongation, %
T6	553	510	17.1
T761	498	430	12.1
RRA	550	507	16.5

The major existing form of chromium in the Al-Zn-Mg-Cu alloy is $Al_{18}Mg_3Cr_2$ phase referred to as the E phase (Ref 22). It is believed that the chromium containing dispersoid particles are formed during solidification and are retained even after solution heat treatment (Ref 23). The dissolution of $Al_{18}Mg_3Cr_2$ particles cannot take place during the retrogression treatment in this investigation. Cilense et al. (Ref 24) also found that the Cr addition to the Al-Zn-Mg-Cu alloy did not change the GP zones retrogression temperature and the temperature of transition from GP zones to η′ phase.

The microstructures of the alloy in T761 and RRA conditions are shown in Fig. 4 as triplanar optical micrographs illustrating the grain structures in the three orthogonal directions of the plate. The microstructures in both conditions are partially recrystallized with fairly large recrystallized grains that were flattened and elongated in the longitudinal direction. The RRA-treated sample exhibits a much larger recrystallized grain structure.

3.2 Fatigue Fracture Behavior

The variation of crack propagation rate (da/dN) with stress intensity factor range (ΔK) of the alloy in T761 and RRA conditions at R = 0.1 and 10 Hz is revealed in Fig. 5, and three regimes of FCP can be identified. RRA-treated sample exhibits high FCP threshold value, as arrowed in Fig. 5. In Paris regime some deviation between the two curves was observed, where the T761-treated sample showed high crack propagation rate whereas the higher resistance against slow crack propagation was observed for the RRA-treated sample. The fatigue fracture of RRA-treated sample occurred ultimately at about ΔK of

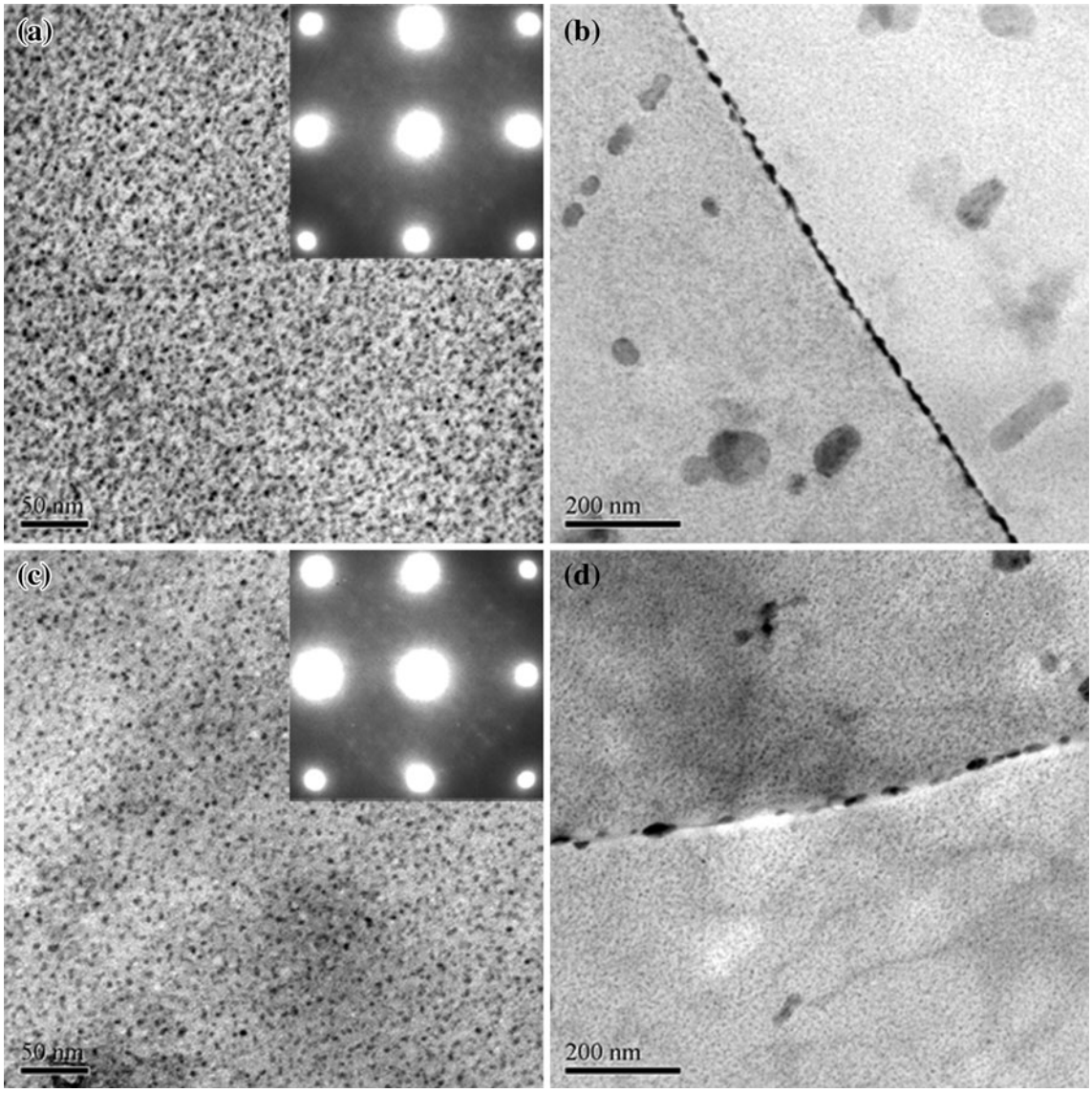

Fig. 2 TEM micrographs and corresponding SAED patterns of the alloy in various conditions. (a, b) T6 and (c, d) retrogressed condition

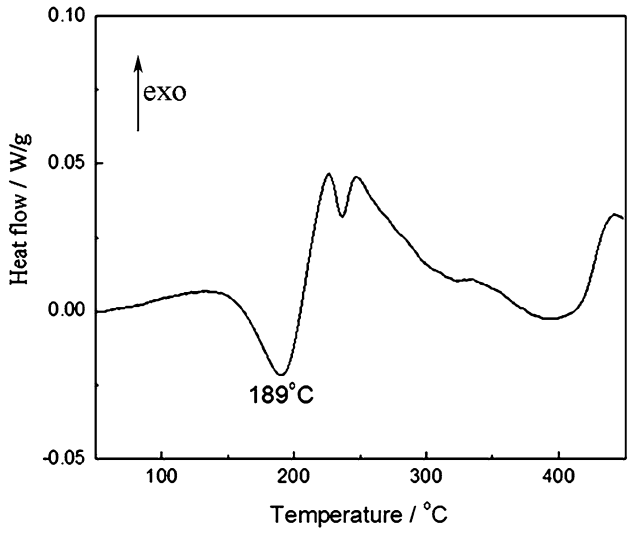

Fig. 3 DSC scan carried out on the Al-Zn-Mg-Cu alloy in T6 condition

28 Mpa $\cdot m^{1/2}$ which is much greater than that in T761-treated sample (about 15 Mpa $\cdot m^{1/2}$). Apparently, the FCP resistance of the RRA-treated sample is higher than that of the T761-treated ones.

Misorientation distributions of grains in both conditions near crack tip at high ΔK regime are illustrated in Fig. 6. Intergranular crack propagation at crack tip and crack branching are observed in T761-treated sample, as shown in Fig. 6(a). It can be clearly seen that the propagation direction of the crack branching is vertical to the loading direction, whereas main crack tends to propagate along grain boundary. In the RRA-treated sample, transgranular crack propagation is observed at crack tip, as circled in Fig. 6(b). Apparently, the intergranular crack propagation exhibits less resistance compared with the transgranular crack propagation arising from the fact that grain boundary is weaker than matrix due to the presence of PFZs. Crack branching is usually recognized as an acceptable method of retarding crack propagation, since it results in a lowering effective stress intensity at crack tip (Ref 25). At high ΔK levels approaching rapid unstable crack growth regime, however, the

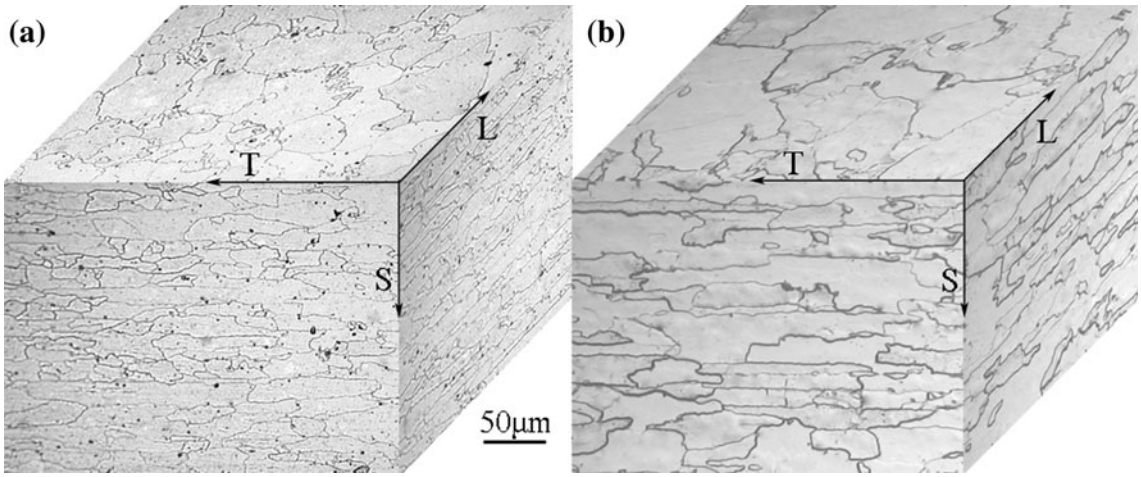

Fig. 4 Triplanar optical micrographs illustrating the grain morphology of the alloy in various conditions. (a) T761 and (b) RRA

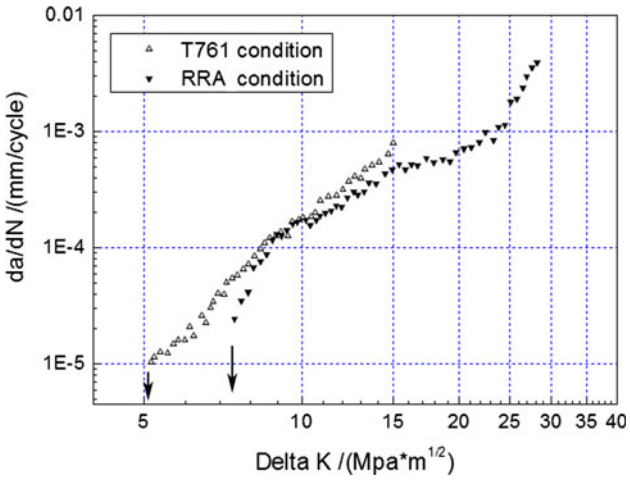

Fig. 5 Fatigue crack propagation rate as a function of stress intensity factor range of the alloy in T761 and RRA conditions

crack propagates at even faster rate and the retarding role of crack branching appears to be relatively less significant. Considering the difference in width of PFZs, as shown in Fig. 1(b) and (d), it is reasonable to conclude that FCP behavior is strongly influenced by the characteristic of grain boundary.

Examination of the fatigue fracture surfaces of samples in both conditions was carried out for comparisons at low magnification to clarify the overall fatigue fracture morphology of different regimes and high magnification to identify the characteristics of the FCP and the fine scale fatigue fracture features. Representative fatigue fracture features are shown in Fig. 7 and 8.

The near-threshold fatigue fracture surfaces of samples in both conditions are given in Fig. 7, indicating the absence of a stage I crystallographic FCP mode. The surfaces for each sample show transgranular fracture. For low ΔK levels, the crack propagates on multiple facets that are at different angles with respect to each other. In T761-treated sample, small facets are observed in Fig. 7(c), whereas the presence of some flat large facets is noticed in RRA-treated sample, as arrowed in Fig. 7(d). The differences in facet appearances might be caused by differences in accumulated plastic strain level between the matrix and the slip bands during fatigue loading (Ref 26).

Figure 8 shows the representative fatigue fracture features of samples in both conditions in Paris regime. Many fatigue plateaus are clearly observed, joined by tear ridges on the fracture surfaces as can be seen in Fig. 8(a) and (b). These relatively smooth plateaus consist predominantly of transgranular crack propagation containing fairly well-defined fatigue striations with the evidence of some secondary cracking. High-magnification images of the fracture surfaces shown in Fig. 8(c) and (d) illustrate the characteristics of fatigue striations and secondary cracks. Apparently, the propagation direction of secondary cracks is nearly perpendicular to the principal crack propagation direction. It is worth of noting that the presence of arrays of secondary cracks in a much higher density is visible in the RRA-treated sample as compared with the T761-treated ones. In the case of the RRA-treated sample, moreover, the spacing of adjacent secondary cracks appears to be uniform, as shown in Fig. 8(d). The formation of more secondary cracks leads to a more complex crack propagation path during fatigue, thereby reducing the fatigue crack driving force and enhancing the crack propagation resistance, is responsible for the lower FCP rate in Paris regime (Ref 27). For the T761-treated sample, secondary crack is found to propagate along the grain boundary as marked by rectangle in Fig. 8(c), which is associated with the higher FCP rate. Some cavities are presented on the grain boundary marked by circles because of the desquamation of GBPs. Also, some fatigue striations are tore at grain boundary resulting in the formation of secondary cracks as arrowed in Fig. 8(c).

The fatigue striation distances of both samples were measured at the same ΔK of 13 Mpa $\cdot m^{1/2}$, as shown in Fig. 9. The striation distance in T761-treated sample is greater than that in RRA-treated ones. For cyclic loads, it has been found that the spacing between adjacent striations correlates with the average crack growth rate per cycle (Ref 28). Therefore, the narrow fatigue striation distance shown in Fig. 9(b) indicates the low FCP rate in RRA-treated sample, as revealed in Fig. 5.

4. Discussions

According to the previous studies (Ref 29-31), several factors influence the near-threshold FCP, like the nature of precipitates and grain size. In the T761-treated sample, there is

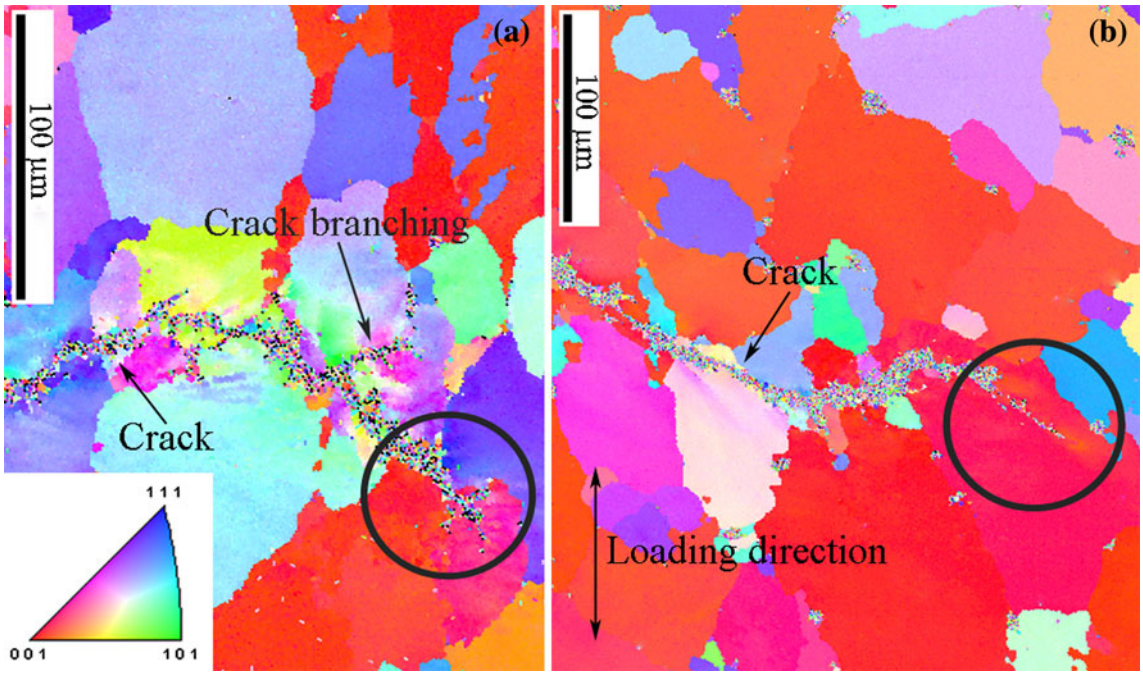

Fig. 6 Fatigue crack propagation paths at high ΔK regime of the alloy in various conditions. (a) T761 and (b) RRA (crack propagation from left to right)

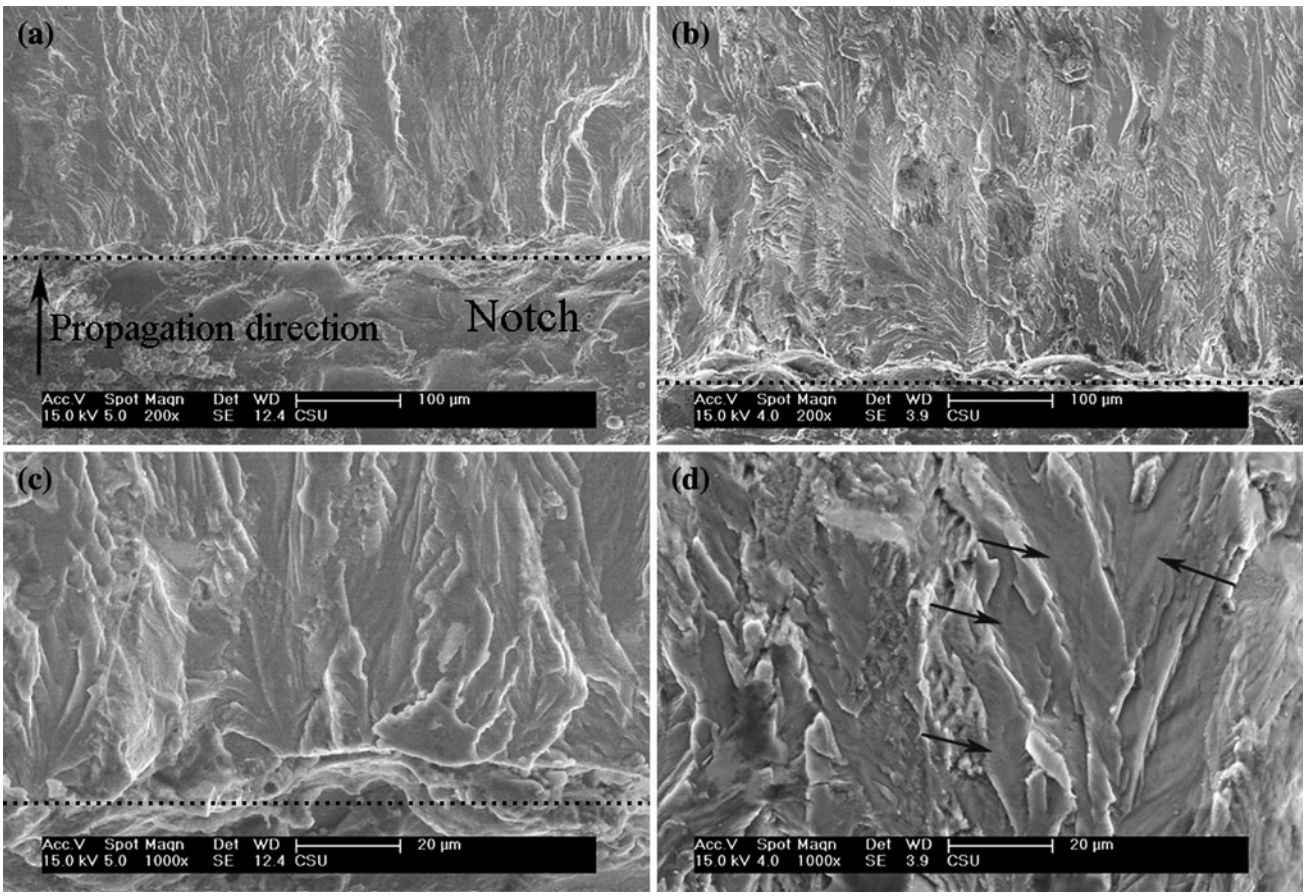

Fig. 7 SEM fractographs in near-threshold regime of the alloy in various conditions. (a, c) T761 and (b, d) RRA (crack propagation from bottom to top)

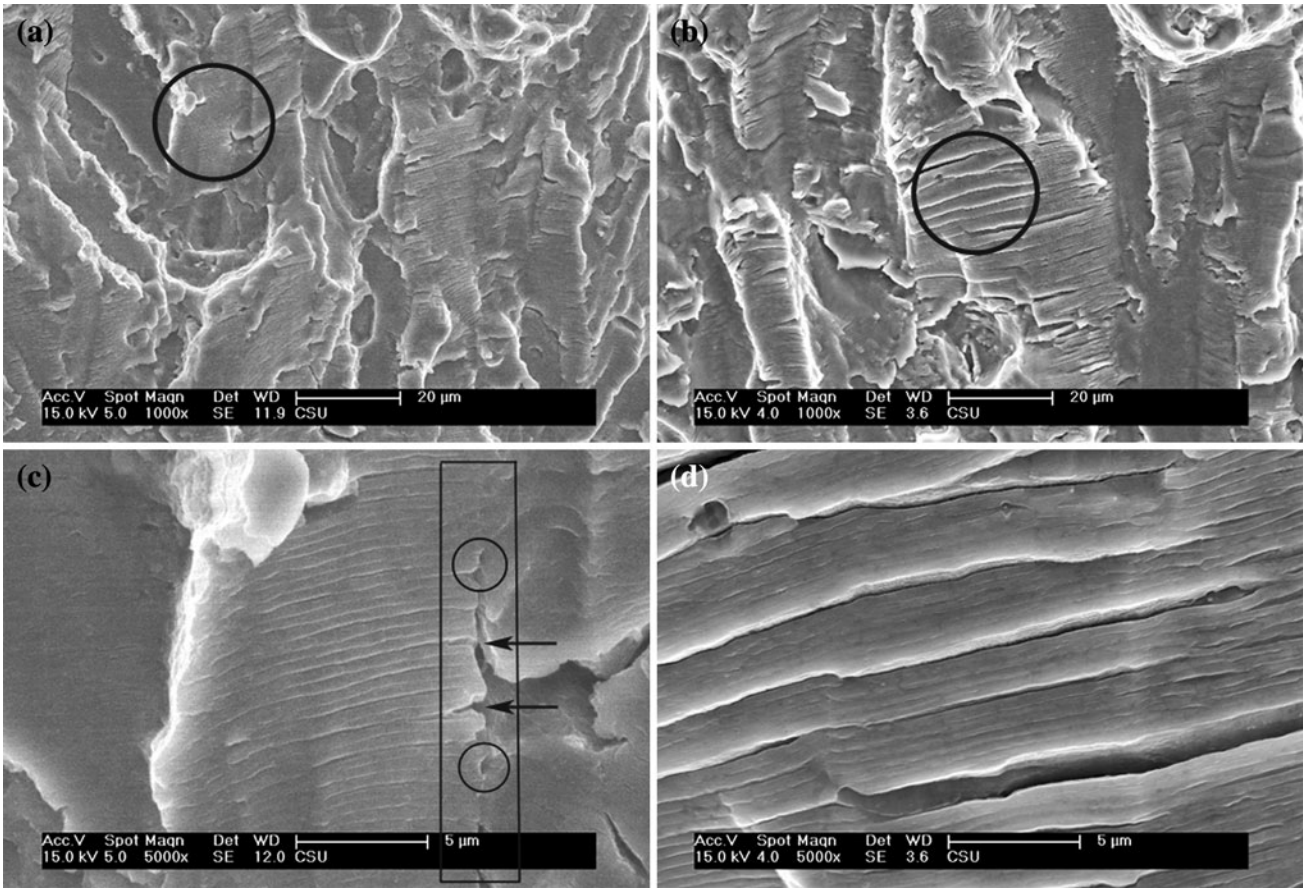

Fig. 8 SEM fractographs in Paris regime showing fatigue striations and secondary cracks. (a, c) T761 and (b, d) RRA (crack propagation from bottom to top)

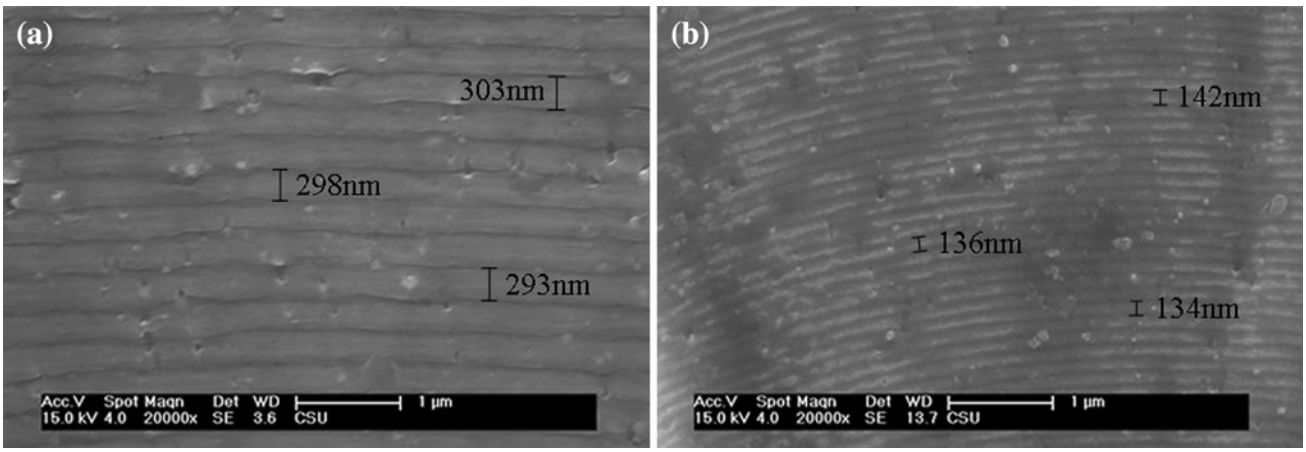

Fig. 9 Fatigue striation morphology of both samples at the same ΔK of 13 Mpa $\cdot m^{1/2}$. (a) T761 and (b) RRA (crack propagation from bottom to top)

a distinct coarsening of the η′ precipitates within the matrix, as can be seen in Fig. 1(a). Fine η′ precipitates and GP zones are able to be shearable by dislocations during fatigue cyclic loading, as proposed by Desmukh et al. (Ref 19). In contrast, a major population of the much coarser η′ precipitates in the overaged sample would be unshearable in nature (Ref 19, 32). At low ΔK levels in near-threshold regime, stage I (shear mode)-type crack propagation mechanism is preferred because the plastic zone is typical smaller than a grain size (Ref 33). The fine η′ precipitates and GP zones in RRA-treated sample are mainly sheared by dislocations promoting planar slip conducing to a higher roughness due to an extensive crack deflection. This leads to zigzag crack morphology, with the deflections occurring over distances of the order of a characteristic microstructural dimension. In addition, the occurrence of persistent slip bands (PSBs) is beneficial to the fatigue crack

growth properties. During fatigue cyclic loading, the kinematical reversibility of cyclic slip may be enhanced by PSBs reducing damage accumulation. Furthermore, PSBs promote crack deflection along a favored slip system which leads to a more tortuous path and contribute to the occurrence of roughness-induced crack closure (RICC). Although other crack closure mechanisms are known to occur, such as plastically induced crack closure (PICC), considering the fact that the plastic zone is really small in near-threshold regime, RICC rather than PICC is the dominant crack closure mechanism in this stage. In the case of the T761-treated sample, the coarse η′ precipitates promote homogeneous deformation through Orowan-type dislocation looping or bypassing of the precipitates. The formation of unshearable precipitates in T761 condition is believed to result in a lower extent of crack deflection and roughness. On the other hand, the finer grains of T761-treated sample shown in Fig. 4 are deleterious to the formation of PSBs because grain boundaries act as barriers to slip of PSBs, whereas large grains with planar slip in the RRA-treated sample provided better resistance of crack propagation by enhanced crack closure levels.

The transition of crack propagation from near-threshold regime to Paris regime is coupled with a noticeable change from single slip mechanism to duplex slip mechanism. At higher ΔK levels, the plastic zone at crack tip encompasses many grains (Ref 28). According to Plastic Blunting model (Ref 34), the increment of crack extension per fatigue cycle is envisioned as occurring due to the plastic blunting of crack tip. Crack tip amenable to duplex slip plastically blunts upon the application of tensile stress. If the stress is reversed into compression, the crack tip resharpens only to be blunted again during the next tension sequence. Since the closure of the fatigue crack during compression cannot fully negate the blunting and the attendant crack extension, crack propagation occurs during a fatigue cycle resulting in the formation of fatigue striations, as shown in Fig. 8. The RRA-treated sample containing shearable particles produce less resistance of dislocation motion as compared with that in T761-treated sample containing unshearable precipitates, promoting the formation of extrusion and intrusion of PSBs on crack fracture surface. Therefore, the formation of secondary cracks can be attributed to the stress concentrations at extrusion or intrusion during fatigue cyclic loading. The uniform secondary crack distribution in RRA-treated sample shown in Fig. 8(d) is beneficial to the decrease of crack propagation rate. In the T761-treated sample, unshearable precipitates serve as effective obstacles to dislocation motion on slip plane. The occurrence of the impede motion on primary slip plane leads to alternating shear on another slip plane. When slip bands impinge on grain boundary, local stress concentrations are generated from the pileup of dislocations at the end of slip bands. PFZs will be the preferential site of plastic deformation because of the depletion of solute atoms in grain boundary area which offers less resistance to deformation as compared with the matrix reinforced by precipitates. Thereby the local stress concentrations promote the formation of secondary crack along grain boundary rather than that in grain interior, as shown in Fig. 8(c). In addition, the tearing fatigue striations at grain boundary arrowed in Fig. 8(c) confirm the existence of the local stress concentrations. It should be noted that PFZs are also observed in RRA-treated sample, but the width is much smaller than that in T761-treated ones, as shown in Fig. 1(b) and (d). Based on the argument of Park and Nam (Ref 35), as PFZs become wider, fatigue crack should be initiated more easily. Besides, the response of GBPs to cyclic deformation results in the easy nucleation of cavities on the interface of GBPs, followed by progressive growth of the cavities with continued deformation and giving rise to their coalescence to form a crack. Compared with the wide PFZs in T761-treated sample, therefore, the effect of narrow PFZs in RRA-treated sample on crack propagation is believed to be negligible.

5. Conclusions

In conclusion, coarse η′ precipitates were present in T761-treated sample while fine dispersed η′ precipitates and GP zones were uniformly distributed in RRA-treated ones. Besides, the width of PFZs in T761-treated sample was found to be much greater than that in RRA-treated ones. Compared with T761-treated sample, the enhanced FCP resistance of RRA-treated sample was attributed to the shearable particles in matrix and narrow PFZs.

Acknowledgments

The authors are grateful for the financial support from Nature Science Foundation of China (51171209) and National Key Fundamental Research Project of China.

References

1. A. Deschamps and Y. Bréchet, Influence of Quench and Heating Rates on the Ageing Response of an Al-Zn-Mg-(Zr) Alloy, *Mater. Sci. Eng. A*, 1998, **251**(1–2), p 200–207
2. X.G. Fan, D.M. Jiang, Q.C. Meng, Z.H. Lai, and X.M. Zhang, Characterization of Precipitation Microstructure and Properties of 7150 Aluminium Alloy, *Mater. Sci. Eng. A*, 2006, **427**(1–2), p 130–135
3. J.A. Charles, F.A.A. Crane, and J.A.G. Furness, *Selection and Use of Engineering Materials*, Butterworth Heinemann, Oxford, 1997, p 227–255
4. E.A. Starke, Jr, and J.T. Staley, Application of Modern Aluminum Alloys to Aircraft, *Prog. Aerosp. Sci.*, 1996, **32**(2–3), p 131–172
5. J.-P. Immarigeon, R.T. Holt, A.K. Koul, L. Zhao, W. Wallace, and J.C. Beddoes, Lightweight Materials for Aircraft Application, *Mater. Charact.*, 1995, **35**(1), p 41–67
6. Y.L. Wu, F.H. Froes, A. Alvarez, C.G. Li, and J. Liu, Microstructure and Properties of a New Super-High-Strength Al-Zn-Mg-Cu Alloy C912, *Mater. Des.*, 1997, **18**(4–6), p 211–215
7. B. Cina, U.S.Patent 3856584, December 24, 1974
8. N.C. Danh, K. Rajan, and W. Wallace, A TEM Study of Microstructural Changes during Retrogression and Reaging in 7075 Aluminum, *Metall. Trans. A*, 1983, **14**(9), p 1843–1850
9. J.K. Park, Influence of Retrogression and Reaging Treatments on the Strength and Stress Corrosion Resistance of Aluminum Alloy 7075-T6, *Mater. Sci. Eng. A*, 1988, **103**(2), p 223–231
10. J.K. Park and A.J. Ardell, Effect of Retrogression and Reaging Treatments on the Microstructure of Al-7075-T651, *Metall. Trans. A*, 1984, **15**(8), p 1531–1543
11. F. Viana, A.M.P. Pinto, H.M.C. Santos, and A.B. Lopes, Retrogression and Re-ageing of 7075 Aluminium Alloy: Microstructural Characterization, *J. Mater. Process. Technol.*, 1999, **92–93**, p 54–59
12. S.P. Knight, N. Birbilis, B.C. Muddle, A.R. Trueman, and S.P. Lynch, Correlations between Intergranular Stress Corrosion Cracking, Grain-Boundary Microchemistry, and Grain-Boundary Electrochemistry for Al-Zn-Mg-Cu Alloys, *Corros. Sci.*, 2010, **52**(12), p 4073–4080
13. G.S. Peng, K.H. Chen, S.Y. Chen, and H.C. Fang, Influence of Repetitious-RRA Treatment on the Strength and SCC Resistance of Al-Zn-Mg-Cu Alloy, *Mater. Sci. Eng. A*, 2011, **528**(12), p 4014–4018

14. T. Marlaud, A. Deschamps, F. Bley, W. Lefebvre, and B. Baroux, Evolution of Precipitate Microstructures during the Retrogression and Re-ageing Heat Treatment of an Al-Zn-Mg-Cu Alloy, *Acta Mater.*, 2010, **58**(14), p 4814–4826
15. A.F. Oliveira, Jr., M.C. de Barros, K.R. Cardoso, and D.N. Travessa, The Effect of RRA on the Strength and SCC Resistance on AA7050 and AA7150 Aluminum Alloys, *Mater. Sci. Eng. A*, 2004, **379**(1–2), p 321–326
16. J.F. Li, N. Birbilis, C.X. Li, Z.Q. Jia, B. Cai, and Z.Q. Zheng, Influence of Retrogression Temperature and Time on the Mechanical Properties and Exfoliation Corrosion Behavior of Aluminum Alloy AA7150, *Mater. Charact.*, 2009, **60**(11), p 1334–1341
17. B.B. Verma, J.D. Atkinson, and M. Kumar, Study of Fatigue Behavior of 7475 Aluminum Alloy, *Bull. Mater. Sci.*, 2001, **24**(2), p 231–236
18. J. Lindigkeit, A. Gysler, and G. Lütjering, The Effect of Microstructure on the Fatigue Crack Propagation Behavior of an Al-Zn-Mg-Cu Alloy, *Metall. Trans. A*, 1981, **12**(9), p 1613–1619
19. M.N. Desmukh, R.K. Pandey, and A.K. Mukhopadhyay, Effect of Aging Treatments on the Kinetics of Fatigue Crack Growth in 7010 Aluminum Alloy, *Mater. Sci. Eng. A*, 2006, **435–436**, p 318–326
20. T.S. Srivatsan, S. Anand, S. Sriram, and V.K. Vasudevan, The High-Cycle Fatigue and Fracture Behavior of Aluminum Alloy 7055, *Mater. Sci. Eng. A*, 2000, **281**(1–2), p 292–304
21. J.Z. Chen, L. Zhen, S.J. Yang, and S.L. Dai, Effects of Precipitates on Fatigue Crack Growth Rate of AA 7055 Aluminum Alloy, *Trans. Nonferrous Met. Soc. China*, 2010, **20**(12), p 2209–2214
22. R. Ayer, J.Y. Koo, J.W. Steeds, and B.K. Park, Microanalytical Study of the Heterogeneous Phases in Commercial Al-Zn-Mg-Cu Alloys, *Metall. Trans. A*, 1985, **16**(11), p 1925–1936
23. W.F. Smith and N.J. Grant, Effect of Chromium and Copper Additions on Precipitation in Al-Zn-Mg Alloys, *Metall. Trans.*, 1971, **2**(5), p 1333–1340
24. M. Cilense, W. Garlipp, A.T. Adorno, and C.S. Lourenço, Influence of the Heat Treatment and of the Chromium Addition on the Precipitation Phenomena of Al-Zn-Mg-Cu Alloy, *J. Mater. Sci. Lett.*, 1985, **14**(4), p 232–234
25. S. Suresh, A.K. Vasudevan, M. Tosten, and P.R. Howell, Microscopic and Macroscopic Aspects of Fracture in Lithium-Containing Aluminum Alloys, *Acta Metall.*, 1987, **35**(1), p 25–46
26. V.K. Gupta and S.R. Agnew, Fatigue Crack Surface Crystallography near Crack Initiating Particle Clusters in Precipitation Hardened Legacy and Modern Al-Zn-Mg-Cu Alloys, *Int. J. Fatigue*, 2011, **33**(9), p 1159–1174
27. S. Bai, Z.Y. Liu, Y.T. Li, Y.H. Hou, and X. Chen, Microstructures and Fatigue Fracture Behaviors of an Al-Cu-Mg-Ag Alloy with Addition of Rare Earth Er, *Mater. Sci. Eng. A*, 2010, **527**(7–8), p 1806–1814
28. S. Suresh, *Fatigue of Materials*, Cambridge University Press, Cambridge, 1998, p 335–342
29. K.T. Venkateswara Rao and R.O. Ritchie, Effect of Prolonged High-Temperature Exposure on the Fatigue and Fracture Behavior of Aluminum-Lithium Alloy 2090, *Mater. Sci. Eng. A*, 1988, **100**, p 23–30
30. P.J.E. Forsyth and A.W. Bowen, The Relationship Between Fatigue Crack Behavior and Microstructure in 7178 Aluminum Alloy, *Int. J. Fatigue*, 1981, **3**(1), p 17–25
31. K. Minakawa, G. Levan, and A.J. Mcevily, The Influence of Load Ratio on Fatigue Crack Growth in 7090-T6 and IN9021-T4 P/M Aluminum Alloys, *Metall. Trans. A*, 1986, **17**(10), p 1787–1795
32. B. Sarkar, M. Marek, and E.A. Starke JR, The Effect of Copper Content and Heat Treatment on the Stress Corrosion Characteristics of Al-6Zn-2Mg-xCu Alloys, *Metall. Trans. A*, 1981, **12**(11), p 1939–1943
33. S. Suresh, Fatigue Crack Deflection and Fracture Surface Contact: Micromechanical Models, *Metall. Trans. A*, 1985, **16**(1), p 249–260
34. C. Laird and G.C. Smith, Crack Propagation in High Stress Fatigue, *Philos. Mag.*, 1962, **7**(77), p 847–857
35. D.S. Park and S.W. Nam, Effect of Precipitate Free Zones on Low Cycle Fatigue Life of Al-Zn-Mg Alloy, *Mater. Sci. Technol.*, 1995, **11**(9), p 921–925